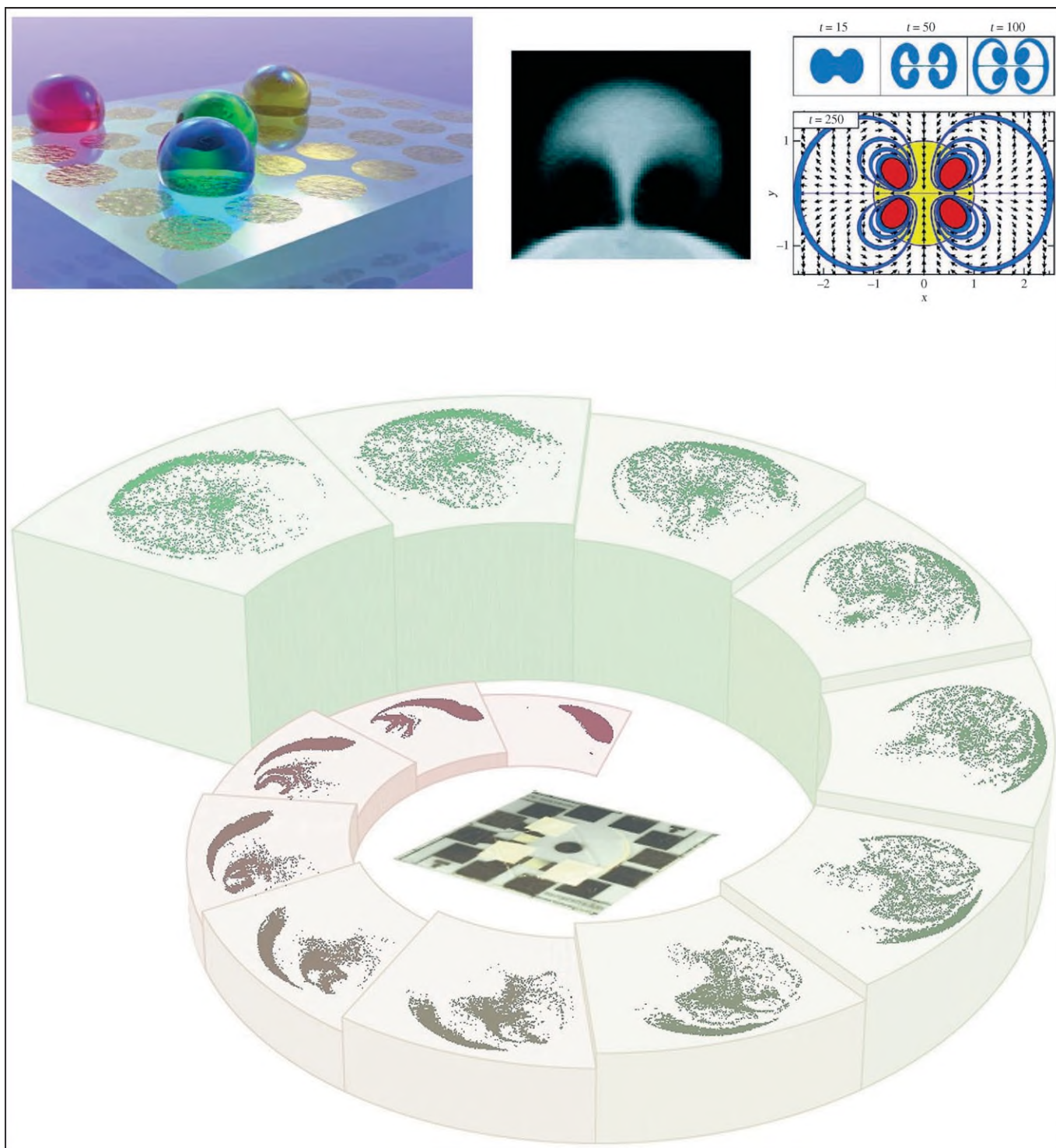


# Microfluidics for Miniaturized Laboratories on a Chip

Thomas A. Franke<sup>[b]</sup> and Achim Wixforth<sup>\*[a]</sup>



*Microfluidic systems promise solutions for high throughput and highly specific analysis for biology, medicine and chemistry while consuming only tiny amounts of reactants and space. On these lab-on-a-chip platforms often multiple physical effects such as electrokinetic, acoustic or capillary phenomena from various disciplines are exploited to gain the optimal functionality. The fluidics on these small length scales differ significantly from our experience of the macroscopic world. In this Review we survey some*

*of the approaches and techniques to handle minute amounts of fluid volumes in microfluidic systems with special focus on surface acoustic wave driven fluidics, a technique developed in our laboratory. Here, we outline the basics of this technique and demonstrate, for example, how acoustic mixing and fluid actuation is realized. Furthermore we discuss the interplay of different physical effects in microfluidic systems and illustrate their usefulness for several applications.*

## 1. Introduction

About a decade ago, a handful of researchers began discussing an intriguing idea. Could the equipment needed for everyday chemistry and biology procedures be shrunk to fit onto a chip the size of a fingernail? Miniature devices for, say, analyzing DNA and proteins should be faster and cheaper than conventional versions. "Lab-on-a-chip" is an advanced technology that integrates a microfluidic system on a micro-scale chip device. The "laboratory" is created by means of channels, mixers, reservoirs, diffusion chambers, integrated electrodes, pumps, valves and more. With this technology, complete laboratories can be created on a square centimeter.

The goal of the lab-on-a-chip technology is to automate standard laboratory processes and to conduct chemical and biochemical analysis in a miniaturized format. The speed and cost-efficiency, combined with small reagent consumption and less waste generation are obvious advantages. Moreover, the results of research can be obtained within a few seconds, instead of hours or days.

The recent development of microfluidic systems marks a rebirth of the old discipline of hydrodynamics, albeit on a much smaller scale than what we are familiar with in our daily lives. Hence, the laws of hydrodynamics still apply, but need to be adjusted to the changed physical environment of the micro-scale. The regime of microfluidics is governed by strong interactions between the fluid and the outer world, be it containers, tubes, or trenches. Here, surface effects like wettability, surface tension, adhesion and cohesion, and others lead to a completely different fluid behavior than that we are used to. Usually, this new behavior is physically described by the ratio of inertial terms and viscous terms in the equations of motion of a fluid volume element—the Reynold's number. Flow at low Reynolds numbers in the macroscopic world is usually restricted to very viscous fluids, like ice in a glacier, for example. Low Reynolds numbers are related to laminar flow and a lack of turbulence, which has enormous consequences for (bio)chemical reactions, for example. Interestingly, the micro-scale behavior of fluids and particles therein is not that unusual even in our macroscopic world, considering that the vast majority of living species on our planet, such as bacteria, have a size of only a few microns. They live in a world where the classical laws of hydrodynamics are not really applicable. In a famous paper, Purcell describes the faith of such microbes in a microfluidic environment,<sup>[1]</sup> describing all the obstacles these creatures experience as compared to an average-sized fish, for example,

but also outlining the strategies live developed to be comfortable in the microscopic world nonetheless.

Microfluidic systems miniaturize chemical and biological laboratory processes to a sub-millimeter scale. Reducing the dimensions of macroscopic biological or chemical laboratories is advantageous, as the small scale allows for the integration of various processes on one chip—analogue to integrated microelectronic circuitry. Also, the reagent volumes required are reduced, which saves material costs and allows the reactions to be carried out at high sample concentrations. These high concentrations drive the reactions towards the products' side and accelerate the kinetics. Finally, miniaturization results in enhanced precision by providing homogenous reaction conditions.

Several approaches to realize microfluidic systems have been reported in the literature. In this context, the term "lab-on-a-chip" has emerged, already outlining the use and typical applications of such systems. In most cases the reagents are moved in channels or capillaries with typical diameters ranging from 10  $\mu\text{m}$  to 500  $\mu\text{m}$ . These channels can be fabricated by deep etching processes on appropriate substrates such as glass, quartz or silicon.<sup>[2]</sup> Alternatively, hot embossing is used to structure polymeric substrates. The channels are capped by anodic bonding or glue processes. Generally, these systems do not allow the reagents to be handled separately, as the channels need to be completely filled in order for the fluidics to work properly. Therefore, the application of these systems is restricted to continuous flow processes rather than batch processes as found in macroscopic laboratories.

The different pumping mechanisms are even more varied than the substrate materials employed in microfluidics. Some pumping units are not an integral part of the chip and must

[a] Prof. Dr. A. Wixforth  
University of Augsburg  
Universitätsstr. 1, 86159 Augsburg (Germany)  
Fax: (+49)821-5983227  
E-mail: achim.wixforth@physik.uni-augsburg.de

[b] Dr. T. A. Franke<sup>†</sup>  
University of Augsburg  
Experimental Physics I, Microfluidics Group  
Universitätsstr. 1, 86159 Augsburg (Germany)

[<sup>†</sup>] Current address:  
Experimental Soft Condensed Matter Group  
School of Engineering and Applied Sciences/Department of Physics  
Harvard University, 40 Oxford St, Cambridge MA 02138 (USA)

be linked with appropriate tubes or pipes. For example, piezoelectric actuation or mechanically moving parts are used to drive the reagents through the channels. Others take advantage of the small dimensions of the microfluidic channel itself.<sup>[3]</sup> As the chemical potentials of the channel walls and the liquid inside differ considerably, a space charge region forms at the interface. A voltage applied along the channel induces a flow at the space charge region which drags along the liquid closer

Thomas Franke studied physics at the University in Göttingen and accomplished his diploma thesis at the Max Planck Institute of Biophysical Chemistry. He completed his Ph.D. thesis at the Max Planck Institute of Colloids and Interfaces and received his Ph.D. in 2004. He then went to the University of Ulm as a postdoc and joined the Dynamics of Complex Fluids group at the Max Planck Institute for Dynamics and Self-Organization in Göttingen.



Since 2005 he is a research group leader at the chair of experimental physics at the University in Augsburg. At present he is on sabbatical at Harvard University, School of Engineering and Applied Sciences in Cambridge, USA. His research interests include microfluidics, cell mechanics and complex fluids.

Achim Wixforth graduated in physics at the University of Hamburg, Germany, where he received his PhD in 1987. He spent a postdoctoral leave at the University of California, Santa Barbara, where he cooperated with Profs. Gosard, Kroemer, and Petroff as an Assistant Research Engineer. Back to Germany, he received his "Habilitation" from the University of Munich in 1994 where he was senior scientist and lecturer before accepting the chair in



Augsburg. He is author and co-author of more than 170 scientific papers and book chapters and looks back on a long list of invited talks. Amongst a variety of other awards he received the Walter Schottky Prize, one of the most prestigious scientific awards in Germany, in 1998 for solid state research, and in 2003 he received the 1st BioTrends Award. Presently, he is full professor for experimental physics at the University of Augsburg, Germany. There, his research efforts include semiconductor nanophysics and nanotechnology, material science, microfluidics and biophysical topics. Prof. Wixforth is a founder of Advalytix AG, Brunntal, Germany, a spin-off company of the Center for NanoScience (CeNS) of the University of Munich. Advalytix has recently been acquired by Olympus Life and Material Science, Europe. He is member of APS, DFG, IEEE, CeNS, and the German Initiative of Excellence "Nano-initiative Munich (NIM)" and serves as a referee for prestigious funding agencies and scientific peer review journals.

to the center of the channel. This electrokinetic effect works only for narrow channels and relatively high voltages. Fluidic motion can also be induced by spatially modulating the wetting properties of a substrate. For aqueous solutions, this can be achieved by patterning the substrate with hydrophobic and hydrophilic regions. The techniques used to realize such a modulation of the wetting properties include micro-contact printing,<sup>[4]</sup> vapor deposition, and photolithography.<sup>[5,6]</sup> Aqueous solutions prefer to cover the hydrophilic regions and avoid residing on the hydrophobic areas. Guided flow can be achieved<sup>[7]</sup> by changing the wetting properties with time. For example, illumination can induce a guided motion of liquids as the free energy of the surface changes locally under illumination.<sup>[8]</sup> Other pumping mechanisms include peristaltic pumps based on thin membranes,<sup>[9]</sup> or polymer films<sup>[10]</sup> with controlled deformation, causing guided flow along microchannels.

## 2. Physical Background

Before giving a selection of different examples for the vast field of applications of microfluidic systems in various disciplines, we summarize the fundamental equations, which govern the motion of fluids. For an in-depth description of general hydrodynamics, we refer to the excellent textbooks of Landau<sup>[11]</sup> and ref. [12]. In ref. [13], the reader can find a summary of physical aspects and applications more focused on microfluidics. Other selected recent reviews are refs. [14, 15]. Generally, the starting point is the continuum hypothesis, that is, we consider an infinitesimal fluid volume element that is small in comparison to the characteristic dimensions of the object of interest, but still large with respect to intermolecular distances. For example, a characteristic length can be the diameter of a capillary of a blood vessel or the width of a microfluidic channel. The scales of both upper and lower limits differ significantly for most applications. For gases at low pressures, however, this consideration might fail and therefore the concept of an infinitesimal volume or "fluid particle" makes no sense anymore. The kinematics of such a fluid particle can be described mathematically with the help of the vector  $\vec{v} = \vec{v}(x, y, z, t)$  representing the velocity of the fluid at a position  $\vec{r} = (x, y, z)$  at time  $t$ . The streamlines of the fluid are connecting lines of the velocity field at a given time  $t_0$ . Their tangents in every point  $\vec{r}$  coincide with the velocity vector  $\vec{v}$ . The motion of a particular fluid particle along its path with respect to the time is called its trajectory. In the case of stationary flow where the velocity does not depend explicitly on time, trajectories and streamlines are identical.

For a fluid we can write down the equation of motion of a fluid particle of mass  $m = \rho dV$  in analogy to Newton's law of motion  $\vec{F} = m\vec{a}$ .

The forces on such a volume element are either acting through its surface or are external volume forces. The former ones give rise to the concept of stress. In this case, an area element  $dA$  experiences forces from both sides. This force per unit area is the stress  $\vec{\sigma}$  and is represented by a second-order tensor. Its components depend on the orientation of the area and the force. Both quantities are vectors, that is,  $\sigma_{xy}$  is the  $x$ -

component of the force on a unit area, with the normal pointing in the  $y$ -direction. The dimension of  $\sigma_{xy}$  is consequently a force per area while the volume force  $\vec{f}$  is force per volume. Therefore the overall force per volume acting on the fluid element yields  $\nabla \vec{\sigma} + \vec{f}$  and due to the fact that Newton describes the total derivative of the velocity as in Equation (1):

$$\rho \left( \frac{\partial \vec{v}}{\partial t} + \vec{v} \cdot \nabla \vec{v} \right) = \nabla \vec{\sigma} + \vec{f} \quad (1)$$

The left-hand side contains the kinematics; we have split the acceleration along a trajectory into a term containing the time dependence of  $\vec{v}$  at a fixed position and another term for the variation due to the flow of the fluid. Note that this term is a scalar product of  $\vec{v}$  and the nabla-operator  $\nabla$  and therefore when applied to  $\vec{v}$ , includes the variation of each component of  $\vec{v}$  as a result of the motion along the three directions of the trajectory. On the right-hand side, the first term is the divergence of the stress tensor, which itself is a vector.

Let us have a closer look at the stress tensor. Consider hydrostatic pressure acting on a volume element  $dV$ . Then, every unit area surrounding this volume experiences the same force directing normal and inwards of this area  $dA_i$ , for example,  $-pdA_i$ . In terms of the stress tensor, this force equals  $\sigma_{ik}dA_k$ . Therefore, we see that the stress tensor only has non-vanishing diagonal elements which all equal  $p$ . This reflects the fact that the hydrostatic pressure is isotropic and acts normal to any surface.

As suggested by this example, we may decompose the stress tensor in two parts, shown by Equation (2):

$$\sigma_{ik} = \sigma'_{ik} - p\delta_{ik} \quad (2)$$

The first term on the right-hand side in general also contains non-diagonal elements which do not vanish. It is this term that drives the relative motion of neighboring volume elements and therefore is called the viscous stress tensor. The derivation of the general form of the viscous stress tensor is lengthy and can be found elsewhere. In Equation (3), we assume the case of an incompressible fluid:

$$\nabla \cdot \vec{v} = 0 \quad (3)$$

and take into account only velocity differences up to the first order. Then, the viscous stress tensor can be written as Equation (4):

$$\vec{\sigma} \propto \eta \nabla \vec{v} \quad (4)$$

If we use this expression and combine it with Equation (1), we obtain the Navier–Stokes equation for an incompressible, Newtonian fluid in its common form, given by Equation (5):

$$\rho \left( \frac{\partial \vec{v}}{\partial t} + \vec{v} \cdot \nabla \vec{v} \right) = -\nabla p + \eta \Delta \vec{v} + \vec{f} \quad (5)$$

Generally, this equation of motion can not be solved analytically, mainly because of its unhandy nonlinear term on the left-

hand side. Fortunately for many problems relevant in microfluidics, this term can be neglected. First assume a simple argument that applies also in non-microfluidic situations. Consider a one-dimensional streaming of the fluid, that is,  $\vec{v} = (v_x, 0, 0)$ . Exploiting the incompressibility reveals that  $v_x$  only depends on  $y$  and  $z$ , and therefore  $\vec{v} \cdot \nabla \vec{v} = 0$ . Here, the nonlinearity vanished due to the simple geometry of the problem. The small length scales of microfluidic systems also justify why this term can be neglected. Comparing the typical time scales for diffusive momentum transport  $L^2\rho/\eta$  on the one side and convective momentum transport  $L/v$  results a dimensionless number [Eq. (6)]:

$$\text{Re} = \frac{L\rho v}{\eta} \quad (6)$$

This “Reynolds number” therefore denotes the ratio of the inertial to viscous forces. Accordingly, if the Reynolds number is small, viscous forces dominate and inertial forces can be neglected. This implies that the convective derivative, the nonlinear term in the Navier–Stokes Equation [Eq. (5)] can be omitted. We see that not only the small dimension  $L$ —as is the case in microfluidics—but also very small velocities or large viscosities can cause extremely small Reynolds numbers. An example of the latter is given by glaciers, as shown in Figure 1.



**Figure 1.** The motion of a glacier is characterized by a very small Reynolds number. Taking a flow velocity of  $1 \text{ m year}^{-1}$  and a length of the glacier of  $1 \text{ km}$  and a density to viscosity ratio of ice to be  $\rho/\eta \approx 3 \times 10^{-7} \text{ s m}^{-1}$  we estimate the Reynolds number to be  $\text{Re} \approx 10^{-11}$ . The laminar flow can be clearly seen from the streaks of stones, which serve as tracer particles.

In those cases where the above simplification holds, the equation of motion simplifies enormously and is called the Stokes equation [Eq. 7]:

$$\rho \frac{\partial \vec{v}}{\partial t} = -\nabla p + \eta \Delta \vec{v} + \vec{f} \quad (7)$$

Due to its linearity for given boundary conditions, the solution of the Stokes equation is unique. This is not the case for the Navier–Stokes equation [Eq. (5)]! Another remarkable property is its reversibility, as illustrated by a striking experiment of G. I. Taylor (Figure 2).



**Figure 2.** The experiment by G. I. Taylor demonstrates the reversibility of the Stokes equation. A colored droplet is introduced into a highly viscous liquid between two concentric and transparent cylinders (Couette apparatus). When rotating the inner cylinder, the droplet is sheared and therefore smeared. After reversion of the direction of rotation the droplet reassembles again.

Experimentally, however, this reversibility is limited by diffusion. Taking a closer look at the reassembled drop of ink in Taylor’s experiment, one can already observe some smears reflecting the diffusion of ink in the oil. In microfluidic systems, owing to the small dimensions, diffusion might take on an even more dominant role. To estimate the relative importance of diffusion, we again compare typical time scales, that is, the typical time scale of diffusion  $L^2/D$  and the time scale of convection  $L/v$ . This famous ratio is the Péclet number, given by Equation (8):

$$Pe = \frac{vL}{D} \quad (8)$$

The interplay of these two effects can be demonstrated in a simple microfluidic device which is a very useful tool for applications, also called a T-sensor.<sup>[16]</sup> The fluids within two channels are brought together at a T-junction and subsequently flow downstream parallel. If the liquids are miscible, a diffusive zone builds up. From the time scales of diffusion and convection, one can estimate the diffusion zone (diffusion time) to scale with the square root of the convection time or the position downstream the channel, respectively. In Figure 3, a chemical reaction between reactants in the two inlet channels forms a fluorescent complex, thus producing a visible diffusion zone.

This interplay between diffusion and convection, however, can also be utilized for sorting and filtering. The so-called H-filter,<sup>[18,19]</sup> combines fluids of two inlets over a certain exchange distance and drains off gained and excess solutions in different outlets. This concept has for instance been used to separate motile from non-motile sperm cells.<sup>[20]</sup>

In laminar flow, which is typical for the low-Reynolds-number regime, mixing is dominated by diffusion, as already estimated by the Péclet number. However, as we have seen in Figure 3, because of the boundary conditions, a convective mixing term might arise. Consider a small fluorescently dyed volume of fluid in a cylindrical channel. As a consequence of the parabolic flow profile within this channel, this stripe

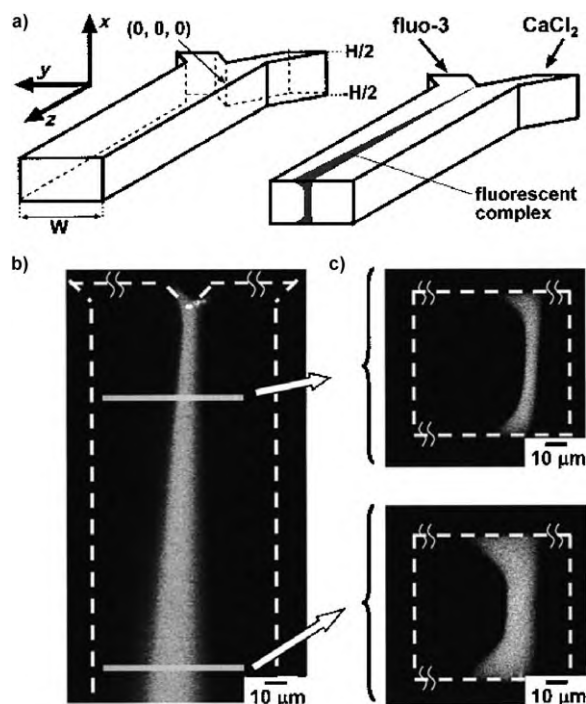


**Figure 3.** Images taken with a confocal microscope reveal significant deviations from the expected square root dependence. Due to the no-slip boundary condition, molecules near the walls spread with  $z^{1/3}$  rather than  $z^{1/2}$  (taken from ref. [17]).

smeared along the flow direction simply because the flow velocity close to the center of the channel is faster than that at the boundaries. On the other hand, on a time scale of  $R^2/D$ , the dye mixes diffusively across the channel with radius  $R$ . An initially thin stripe therefore smears to a length of  $\approx v_{\max}R^2/D$ . This mechanism of convective mixing is called Taylor dispersion.

This concept of mixing can be applied to immiscible fluid systems like water droplets in an oily bulk solution. Here, the diffusive mixing is limited by surface tension, which stabilizes the drops. Pumping these drops through a curved channel, however, results in convective mixing inside the drops (Figure 4).

The concept of using droplets as containers has great potential for high-throughput screening applications where DNA, cells or other reactants are encapsulated. Such droplets can be produced at rates of 10 kHz and in volumes smaller than picoliters. These droplets can subsequently fused or even split into drops of smaller volumes. The T-junction already discussed can be used to split drops into half simply by applying a suitable geometry to direct the fluid flow (see Figure 5).

Such drops can be produced in a co-flowing device. These devices can be built up for example, by using a circular glass capillary, which is inserted into a square capillary. The fluids in both capillaries flow in the same direction and therefore the inner fluid breaks up into droplets at appropriate flow conditions. When the fluid flows at low rates, individual monodisperse drops are formed periodically at the tip of the capillary orifice, in a process termed dripping.<sup>[23,24]</sup> On the other hand, if

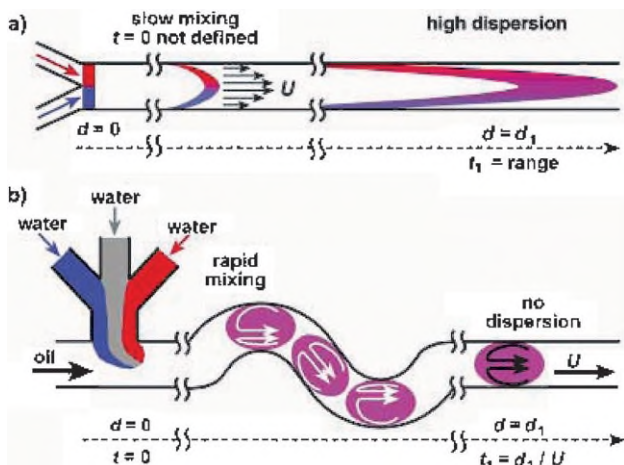


**Figure 4.** a) In a microfluidic channel a dyed region smears into a parabolic shape due to Poiseuille flow. Additionally it smears diffusively across the channel. b) Using immiscible oil prevents the smearing. Mixing can be achieved by using convective motion induced by a curved channel geometry (taken from ref. [21]).

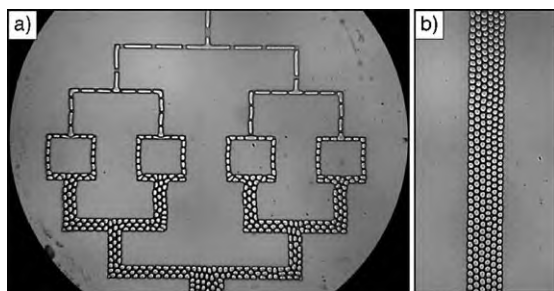


**Figure 5.** a) Sequential breakup of drops at a T-junction. Drops are formed at a highly dispersed phase-volume ratio (not shown) and subsequently broken up to form smaller drops. b) Drop flow downstream building up a hexagonal closed packed order (taken from ref. [22]).

the flow rate is increased above a critical value, a long jet is formed and the drops are generated far downstream. A variation of this principle is a counter-flowing device, where both fluids are introduced from both ends and the inner fluid is hydrodynamically focused (Figure 6).<sup>[25]</sup> One advantage of this geometry is that the size of the drops can be much smaller than the orifice of the micropipette. Recently it was reported that such drop makers can also be manufactured in devices made up of the silicone elastomer PDMS through the use of soft lithography, which offers the opportunity of mass production of such devices.<sup>[27]</sup> Above all, one can extend this idea to create controlled monodisperse double- or even multi-emulsions which contain drops within drops (Figure 7).<sup>[28]</sup> Figure 6 shows a possible design of glass capillaries that can make a double emulsion. Here, co-flowing and flow-focusing devices are used.

It is characteristic for microfluidics that physical effects that typically are of minor relevance in macroscopic hydrodynamics become more important. By only taking into account the smallness of the Reynolds number and considering a Stokes flow, one might naively regard such systems as simple or even boring. Actually, the small size of microfluidic systems gives

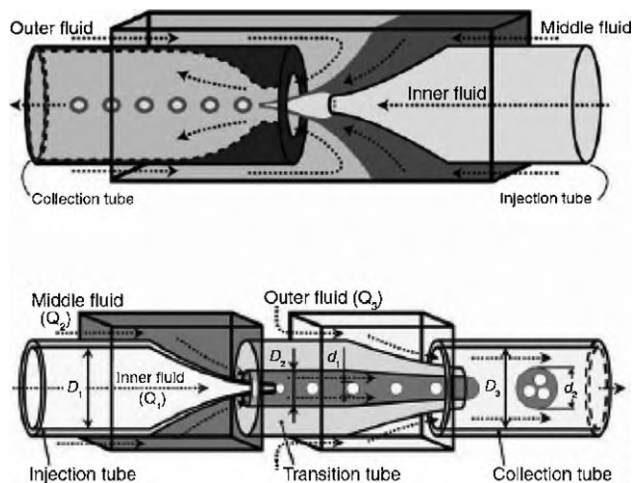


**Figure 6.** Top: Fabrication of a double emulsion in a co-flowing and flow-focusing device (taken from ref. [25]). Bottom: A device with two subsequent co-flowing streams in glass capillaries (taken from ref. [26]).

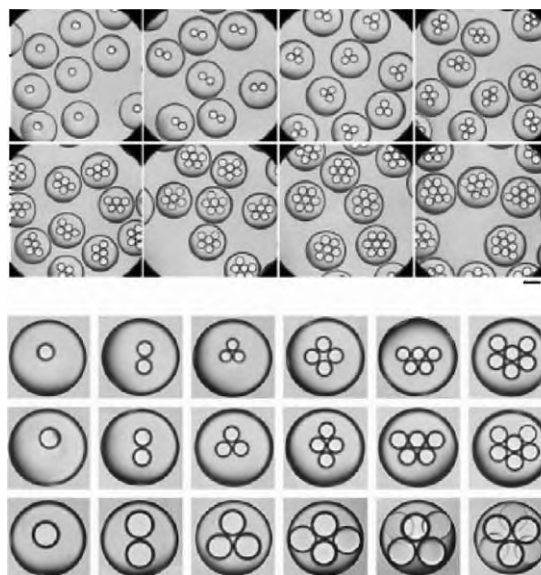


**Figure 7.** Top: Optical micrograph of a monodisperse double emulsion containing a controlled number of monodisperse single emulsion. Bottom: Optical micrograph of double emulsion showing a controlled increase in the diameter of the inner droplets in each column with constant number of inner droplets (taken from ref. [26]).

rise to versatile and complex behavior, because effects such as surface tension or electro-dynamical phenomena become pronounced and are of significant orders of magnitude.

Probably the most well-known example is the formation of a fluid drop. The surface tension  $\sigma$  acts to minimize the surface of the fluid and therefore a spherical shape forms. Apart from the air–fluid interface, the fluid–substrate interface confines the fluid and a spherical cap is formed. Deviations might arise because a body force such as gravity acts on the fluid simultaneously.

The relative importance of surface tension is described by a characteristic length scale, the capillary length  $\lambda_c = \sqrt{\sigma/\rho g}$ . For water, this length is about 2 mm, that is, droplets that are

larger possess significant deviations from the spherical shape. Microfluidic systems are in general smaller and therefore dominated by surface effects. In accordance with the Reynolds and Péclet numbers, a dimensionless number, the Bond number  $Bo = \rho g R^2 / \sigma$ , is generally used to specify this interplay instead of the capillary length. There is a large number of other dimensionless numbers characterizing opposing phenomena of different physical origin. In Table 1 some of the most common numbers are summarized.

**Table 1.** Overview of dimensionless numbers often used in microfluidics to characterize the relative importance of opposing effects (adapted from ref. [15]).

Bond	$Bo = \rho g R^2 / \sigma$	surface tension/gravity
Reynolds	$Re = L\rho v / \eta$	Inertia/viscous
Péclet	$Pe = vL / D$	Convection/diffusion
capillary	$Ca = \eta v / \sigma$	Viscous/interfacial
Deborah	$De = \tau_{\text{polymer}} / \tau_{\text{flow}}$	Polymer relaxation time/flow time
Elasticity	$El = \tau_{\text{polymer}} \eta / \rho h^2$	Elastic effects/inertial effects
Grashof	$Gr = \rho v_b L / \eta$	$Re$ for buoyant flow
Knutsen	$Kn = \beta / L$	Slip length/macrosopic length
Rayleigh	$Ra = v_b L / D$	$Pe$ for buoyant flow
Weissenberg	$Wi = \tau_p \dot{\gamma}$	Polymer relaxation time/shear rate time

The fluid–substrate contact angle  $\theta_{\text{eq}}$ , as measured in the inside of the drop, is given by the equilibrium of the surface tensions between substrate (s), liquid (l), and gas (g). This is the balance of forces defined by Young’s equation [Eq. (9)]:

$$\sigma_{\text{sg}} - \sigma_{\text{sl}} - \sigma \cos \theta_{\text{eq}} = 0 \quad (9)$$

The size of the spherical cap is given by the volume of the fluid. This apparently simple system becomes much more complex when adding a wetting contrast to the substrate, such as a wetting hydrophilic and a dewetting hydrophobic region,<sup>[29,30]</sup> or some  $L$  roughness (Wenzel’s law). Additionally, one might take advantage of another effect called electrowetting. Hereby the contact angle can be varied by applying an external voltage between a drop and an insulated electrode on which the drop is deposited. Upon increasing the voltage, droplets become elongated on a stripe and a new contact angle for electrowetting  $\theta_{\text{ew}}$  is established.<sup>[31]</sup> The Lippmann equation, given by Equation (10), relates  $\theta_{\text{ew}}$  and the applied voltage  $U$ :

$$\cos \theta_{\text{ew}} = \cos \theta_{\text{eq}} + \frac{1}{2} \frac{\epsilon_0 \epsilon}{d \sigma} U^2 \quad (10)$$

Here  $d$  and  $\epsilon$  are the thickness and the dielectric constant of the insulating layer of the electrode, respectively, and  $\epsilon_0$  is the vacuum permeability. In Figure 8 the variation of the morphology of a drop and its contact angle depending on the external voltage is demonstrated.

There is a large number of other applications of electrohydrodynamic effects. Herein, we only mention a few of them,

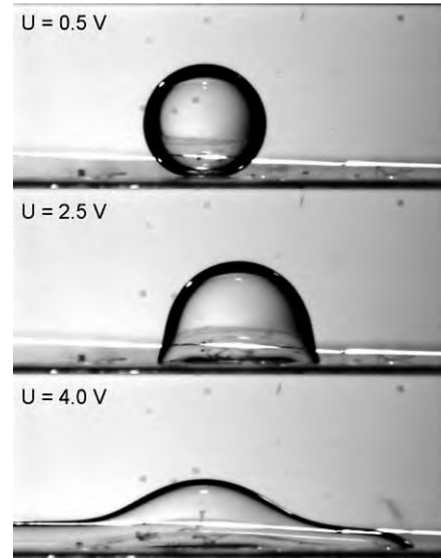


**Figure 8.** Water droplet deposited in oil and attached to an insulating electrode surface at the bottom. According to the voltage between the electrode and the drop the morphology of the drop changes and the contact angle decreases with increasing voltage. This electro-wetting effect can be used for example, to actuate drops on surfaces or to mix reactants in a droplet (photo courtesy of F. Mugele, University Twente). The insets show values of the voltage before amplification. The actual applied voltage is a factor of  $\times 100$  higher.

namely electrophoresis, dielectrophoresis and electro-osmosis. For a more complete and detailed discussion, we refer to the excellent reviews by Squires and Quake<sup>[15]</sup> and Stone et al.<sup>[14]</sup> The effect definitely utilized most often is electrophoresis. This is the motion of a charged particle driven by an electric field in a resting fluid. Nowadays electrophoretic chambers for the separation of different lengths of negatively charged DNA on a gel are basic equipment in every biology lab. The miniaturized version is called capillary electrophoresis (CE). Here the charged objects move along a small capillary tube or a microchannel. Charge objects are characterized by their electrophoretic mobility  $\mu$ . The mobility is the ratio of the migration velocity and the externally applied electric field along which the particle moves,  $\vec{v}_{\text{el}} = \mu \vec{E}$ . Because the particle moves in a liquid, its charge might be shielded if immersed in an electrolyte, as is typically the case for aqueous solutions. In other words, an electric double layer of counter ions encompassing the charge is formed. The thickness of this double layer is given by the Debye–Hückel length,  $\lambda_{\text{DH}}$ . For an aqueous solution containing  $1 \mu\text{M}$  salt, this length is of the order of a few tens of nanometer. Depending on the size of the object, one can derive two estimates for the mobility. First assuming the dimension of the charged object is much smaller than the Debye–Hückel length, the object behaves like in an insulating medium and the mobility is given by the ratio of the charge  $q$  and the Stokes friction,  $\mu = q / 6\pi R \eta$ , with  $R$  the dimension of the object. In contrast, for large particles a double layer forms and the mobility is given by  $\mu = \epsilon \epsilon_0 \zeta / \eta$  where  $\zeta$  is the zeta potential, which describes the effective charge and size of an object surrounded by the diffusive double layer. Therefore, in a CE system, objects can be separated due to their electrophoretic mobility. Often

in such devices, electro-osmosis helps to fight mixing and smearing due to parabolic flow profiles (see Figure 4). The term electro-osmosis describes the motion of an ionized fluid driven by an electric field. To illustrate this effect, consider a capillary or microchannel with charged walls. Glass for example, is typically negatively charged in aqueous solution as it releases protons and  $\text{SiO}^-$  groups are formed. Therefore a diffusive double layer with opposite charge builds up. If an electric field parallel to the channel walls is applied, a body force is acting on the charged double layer. However, the bulk solution is neutral and therefore not affected by the electric field. Hence, one can assume the whole fluid is dragged by the moving layer due to viscous effects. There is a notable relation between the velocity field  $\vec{v}(x)$  along the channel and the parallel acting electric field  $\vec{E}(x)$ . Obviously the electric field has to obey the Laplace equation,  $\nabla^2 \vec{E} = 0$  for the neutral bulk solution. Furthermore the hydrodynamic problem on this length scale has to obey the simplified Stokes equation,  $0 = -\nabla p + \eta \nabla^2 \vec{v}$ . Thus, without an external pressure gradient, a solution of both equations yields the relation  $\vec{v} \propto \vec{E}$  and for an axially applied and constant external electric field this causes a uniform fluid flow known as the plug flow. Thus, there is no smearing of fluid stripes due to a cross-sectional flow profile as in the case of Poiseuille flow (see Figure 4). The last effect that we address in this context is dielectrophoresis, that is, the motion of a neutral object by the application of an electric field gradient. A polarizable object exhibits a dipole if an external electric field is present. The field gradient then acts on the dipole and forces the object towards the region of maximal field strength. Briefly, if one assumes the dipole moment to be proportional to the field  $\vec{p} \propto \vec{E}$  and the potential energy to be  $W \propto \vec{p} \cdot \vec{E}$ , the force acting on a dipole is  $\vec{F} \propto \nabla \vec{E}^2$ . The latter proportionality is given by half the polarizability of the object. There is a useful variation of the dielectrophoretic effect, which is called negative dielectrophoresis. Here the polarizability of the bulk fluid is larger than the particle which is embedded therein. In general, one then has to deal with both the polarizable object and the fluid.

Magnetic effects can also be exploited in order to manipulate objects in fluidic devices.<sup>[32,33]</sup> Super paramagnetic beads of submicron diameters can align to form chains possessing a magnetic dipole moment.<sup>[34,35]</sup> External magnetic fields can then be used to maneuver these chains and, for example, probe the sample for local rheological properties. Recently, a hybrid lab-on-a-chip system was introduced which combines CMOS (complementary metal-oxide-semiconductor) technology and microfluidics and integrates an array of micro-electromagnets onto the chip platform to position magnetic objects laterally (Figure 9).<sup>[36]</sup>

The microfluidic device to maneuver these cells consists of a combination of different technologies and adapts conventional CMOS technology to microfluidics (Figure 10). The integration of complementary techniques is a typical characteristic of this technology and reflects the influence and interplay of different physical phenomena as listed in Table 1.

In the next section we focus on the technological applications and discuss different device designs.

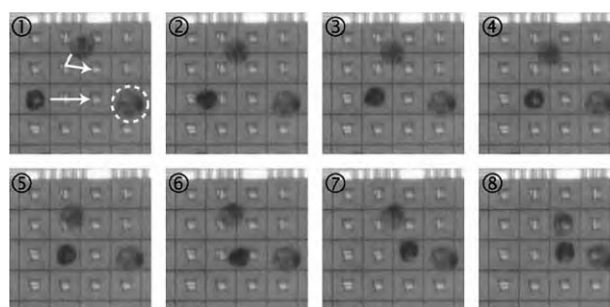


**Figure 9.** BCE cells are magnetically manipulated using the hybrid system. Magnetic beads are taken up by the cells through endocytosis. Three cells are trapped and individually controlled (taken from ref. [37]).

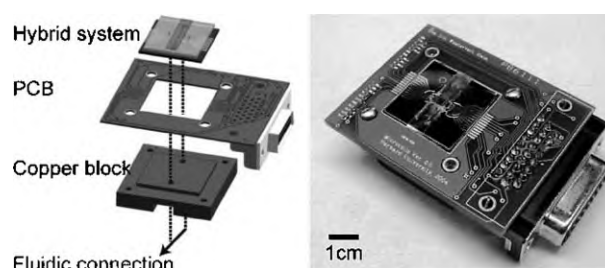


**Figure 10.** CMOS/microfluidic hybrid system for magnetic manipulation on a chip. The CMOS generates microscopic magnet field patterns which are programmable and can be varied at high speed. To enhance biocompatibility, the temperature of the microfluidic channel can be controlled.

### 3. Existing Technologies

Microfluidics hence deals with the handling and manipulation of minute amounts of fluids; volumes thousands of times smaller than a common droplet. Microfluidics means measuring in microliters, nanoliters or even picoliters. The power of the microfluidics field lies at the interfaces between biotechnology, medical industry, chemistry and micro electro-mechanical systems (MEMS). During the past 20 years, microfluidics, micrometer-scale total analysis systems, ( $\mu$ TAS) or lab-on-a-chip devices have revived interest in the scaling laws and dimensionless groups for downscaling purposes.<sup>[38]</sup> Technically, microfluidics already started twenty years ago, principally in inkjet printer manufacturing.

While the earliest reported micro-scale devices consisted of channels etched in solid substrates such as silicon,<sup>[39,40]</sup> glass<sup>[41]</sup> and plastic,<sup>[42]</sup> MEMS fabrication technologies have been increasingly applied to fabricate highly sophisticated devices from a variety of materials, including soft elastomers such as polydimethylsiloxane (PDMS),<sup>[43,44]</sup> with hundreds of microchannels and integrated sensors to measure physiological parameters.

The ability to control precisely parameters such as substrate properties, flow rate, buffer composition and surface chemistry in these micro-scale devices makes them ideally suited for a broad spectrum of cell-biology-based applications ranging from high-throughput screening of single cells and 3D scaffolds for tissue engineering to complex biochemical reactions

like polymerase chain reaction and drug detection. Micro-scale devices offer the possibility of solving system integration issues for cell biology, while minimizing the necessity for external control hardware. Many applications, such as single-gene library screening, are currently carried out as a series of multiple, labor-intensive steps required in the array process, from for example, DNA amplification, reporter molecule labeling and hybridization. While the industrial approach to complexity has been to develop elaborate mechanical high-throughput workstations, this technology comes at a price, requiring considerable expenses, space, and labor in the form of operator training and maintenance. For small laboratories or research institutions, this technology is simply out of reach. Devices consisting of addressable micro-scale fluidic networks can dramatically simplify the screening process, providing a compartmentalized platform for nanoliter aliquots. But making miniature labs is not just a question of scaling down conventional equipment. Nanoliter volumes of liquid behave in curious ways. For example, we are used to seeing liquids mix by turbulent flow, as illustrated by the way cream swirls into coffee. But such turbulence does not occur in closed channel or tubing systems just a few micrometers wide. Streams of liquids flow alongside each other over short distances without mixing. At the other end of the application spectrum, the ability to regulate fluid flow within open micro-scale devices with nanoliter precision has also generated interest in using them as tools for tissue engineering or bionic applications. Advances in substrate micro-patterning techniques to mimic capillaries (e.g. bionic approaches), the implementation of biocompatible and biodegradable substrates, and the ability to pattern surfaces with molecules to simulate cell adhesion have provided researchers with excellent tools to understand complex biophysical processes. An example is the adhesion of von Willebrand factor fibers to stop bleeding under high shear-stress conditions as found in small blood vessels.<sup>[45]</sup>

Several groups have recently reported on the development of nanofluidic systems to mechanically manipulate and isolate single cells or small groups of cells in micro scale tubing and culture systems. The Quake group used multilayer soft lithography, a technology to create stacked 2D micro-scale channel networks from elastomers, to fabricate integrated PDMS-based devices for programmable cell-based assays.<sup>[46]</sup> They applied the micro device for the isolation of single *E. coli* bacteria in subnanoliter chambers and assayed them for Cytochrome C peroxidase activity. Khademhosseini and co-workers reported on the use of polyethylene glycol (PEG)-based micro-wells within micro-channels to dock small groups of cells in predefined locations. The cells remained viable in the array format and were stained for cell surface receptors by sequential flow of antibodies and secondary fluorescent probes.<sup>[47]</sup> Trapping of cells using biomolecules in nanofluidic systems has been demonstrated using antibodies and proteins with high affinities to the target cells.<sup>[48]</sup> Chang et al. used square silicon micro-pillars in a channel coated with the target protein, an E-selectin-IgC chimera, to mimic the rolling and tethering behavior of leukocyte recruitment to blood vessel walls.<sup>[49]</sup> There are certainly many more different examples on recently developed miniatur-

ized systems aiming toward the performance of a true laboratory on a chip, but it would be beyond the scope of this article to account for all of them.

#### 4. Actuation Mechanisms

Micro-pumps are one of the key components in 3D lab-on-a-chip systems. They can be divided in two general categories: mechanical and non-mechanical pumps.<sup>[50]</sup> Mechanical pumps usually utilize moving parts such as check valves, oscillating membranes, or turbines for delivering a constant fluid volume in each pump cycle.<sup>[51]</sup> These are mainly used in macro-scale pumps and micro-pumps with relatively large sizes and flow rates. Since the viscous forces in microchannels increase with the second power of miniaturization, mechanical pumps usually cannot deliver enough pumping power. Non-mechanical pumps add momentum to the fluid for pumping effect by converting another form of energy into kinetic energy and are therefore advantageous at the micro-scale. For flow rates larger than  $10 \text{ mL min}^{-1}$ , miniature pumps or macro-scale pumps are the most common solution. The typical operation range of positive-displacement micro-pumps lies between  $10 \mu\text{L min}^{-1}$  to several  $\text{ml min}^{-1}$ . For flow rates of less than  $10 \mu\text{L min}^{-1}$ , alternative dynamic pumps are needed for accurate control of these small amounts of fluids. With these flow rates, most of the pumps are working in the range of Reynolds numbers between 1 and 100, and therefore in the laminar regime.

Another kind of mechanical pump, the rotary pump, can be realized with micro-machining techniques for pumping highly viscous fluids. Ahn and Allen presented a micro-pump with a micro-turbine as rotor in an integrated electromagnetic motor.<sup>[52]</sup> Doepper and coworkers presented a two-gear wheel rotary pump with a flow rate of  $55 \mu\text{L min}^{-1}$  in  $500 \mu\text{m}$  chamber heights. The gears forced the fluid along by squeezing it to an outlet.<sup>[53]</sup> Centrifugal microfluidic platforms are of particular interest for assay integration as their artificial gravity field intrinsically implements a pumping force as well as an established method for particle separation without actuation, apart from a standard rotary drive. The Zengerle group presented a plasma extraction method from whole blood on a rotating disk with a capillary system for subsequent on-disk processing.<sup>[54]</sup>

Ultrasonic pumping is an alternative gentle pump principle with no moving parts, heat or strong electric field involved. Yang and coworkers designed an active micro-mixer based on ultrasonic vibrations and successfully tested their system using water and uranine.<sup>[55]</sup> The pump effect is caused by acoustic streaming, which is induced by a mechanical traveling wave. The mechanical wave can be a flexural plate wave<sup>[56,57]</sup> or a surface acoustic wave (SAW).<sup>[58,59]</sup> The mechanical waves are excited by interdigital transducers placed on a thin membrane coated with piezoelectric film,<sup>[56,57]</sup> or on a piezoelectric bulk material.<sup>[58,59]</sup> This is an alternative to the electro-wetting based transport of droplets.

All mechanical pumps require a mechanical actuator, which generally converts electric energy into mechanical work.<sup>[60]</sup>

External actuators include electromagnetic actuators with a solenoid plunger and external electric field, disk- or cantilever-type piezoelectric actuators, stack-type piezoelectric actuators, pneumatic actuators and shape memory actuators. The biggest drawback of external actuators is their large size, which restricts the size of the whole micro-pumps. The advantage is the relatively large force and displacement generated by external actuators.

Integrated actuators are electrostatic, thermo-pneumatic, electromagnetic and bimetallic. Despite their fast response time and good reliability, electrostatic actuators cause small forces and very small stroke. Thermo-pneumatic actuators on the other hand, generate large pressures and relatively large strokes. However, they require a large amount of thermal energy for their operation, and consequently, consume a lot of electric power.

Non-mechanical pumps can be divided into electro-hydrodynamic (EHD), electro-kinetic, phase transfer, electro-wetting, electrochemical and magneto-hydrodynamic pumps.<sup>[50,61]</sup> Electrokinetic pumping and particle manipulation principles are based on surface forces and thus gain impact within micro-dimensions, due to the increased surface-to-volume ratio. Hence, they are often employed in lab-on-a-chip applications for the analysis of chemical compounds. The EHD induction pump is based on the induced charge at the material interface. A traveling wave of electric field drags and pulls the induced charge along the wave direction. It was first presented by Bart et al.,<sup>[62]</sup> with similar designs by Fuhr and coworkers.<sup>[63]</sup> A fluid velocity of several hundred microns per second can be achieved with this pump type. In contrast to the EHD pumps, electro-kinetic pumps utilize the electric field for pumping conductive fluids. Electro-kinetic phenomena can be divided into electrophoresis and electro-osmosis. Electrophoresis is the effect by which charged species in a fluid are moved by an electrical field relative to the fluid molecules and is used to separate molecules, such as DNA, depending on the size. In contrast to electrophoresis, electro-osmosis is the pumping effect of a fluid in a channel under the application of an electrical field. Again, we refer the reader to a review article on this subject (see ref. [50]). Instead, we now turn to a somewhat more detailed description of an alternative lab-on-a-chip concept that has recently been developed in our own laboratories. It is based on the concept of acoustic streaming, as generated by the interaction between a surface acoustic wave (SAW) on a solid and a fluid at the surface of the solid.

## 5. Digital Microfluids

Watching a typical chemist or biologist doing his or her work in the laboratory, the first thing that strikes the observer is that they usually operate with discrete fluid volumes. Unlike the fluid handling in a chemical plant, nearly all the fluid handling is hence done in a digital fashion. The reason is obvious. Closed volumes being connected by tubes and hoses (analogous to fluidics) are much more difficult to fabricate, and cross-contamination, intermixing, interdiffusion and similar difficulties are easily avoided. Moreover, the flow resistance in

tubes strongly depends on the liquids actually used, making the precise pumping and dispersion of the liquid a cumbersome task in many cases. A multiply connected network of tubes and hoses represents a complex and very nonlinear system, where changes at one end of the network have a notable impact and crosstalk to the fluid/pressure behavior at the other end.

The digital fluidics approach thus requires small containers of well controlled volume as test tubes on the micro scale. This is where droplet-based fluidic systems enter the scene. Once we have a platform at hand able to control the movement and the handling of small fluid volumes in form of droplets, and we find a way to actuate these droplets deliberately, we have a system that can truly be regarded as a miniaturized version of a macroscopic laboratory. Small droplets serve as virtual micro-scale test tubes and reactor vessels, being completely independent from each other and hence reducing the risk of cross-contamination and intermixing to a minimum. These droplets, if small enough, do not need any containers, as surface tension acts as a potential well holding the fluid in place, as shown in Figure 11.



**Figure 11.** Droplets on a chemically prestructured chip surface. If the droplets are small enough and the surface consists of areas of preferred wettability (hydrophilic anchors), surrounded by hydrophobic regions, the droplets are stabilized at a predetermined volume. They act as individual virtual test tubes for micro-scale laboratories.

In this way, we are able to create flatland analogs to the channels, tubes, reservoirs, mixing chambers and similar building blocks usually employed to guide, contain or process liquids in a fluidic network. By a chemical modification of parts of the chip surface (e.g. silanization employing octadecyltrichlorosilane (OTS) based surface chemistry), we create patterns of preferred wettability (hydrophilic regions), being separated by regions of surface chemistry where fluids are repelled (hydrophobic areas). Employing lithographic techniques borrowed from semiconductor microelectronics, we can thus fabricate completely flat, 2D fluidic networks, where liquids are confined to virtual tracks, reservoirs and reaction chambers by surface tension alone. In Figure 12, we depict some of such self-assembled virtual potential wells for fluids on a surface. Photolithographic techniques have been employed to create containers for the smallest amounts of liquid, having predetermined shapes, such as a hexagon or a tube with a narrowing (acting as a pressure-driven valve). Given this surface functionalization, either closed fluid volumes or single droplets may be acousti-

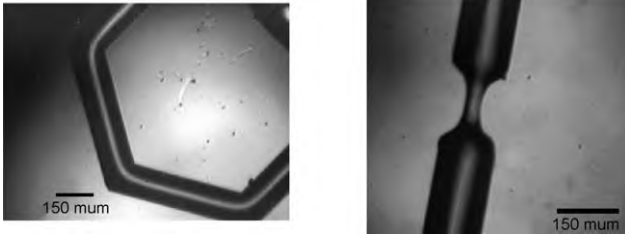


**Figure 12.** Photolithographically defined surface modification to modulate its wettability. This way, virtual fluidic tracks are created to confine small amounts of liquid to predetermined geometries or to guide a SAW-driven droplet along a predetermined path on the chip surface.

cally guided along predetermined pathways along the surface of the chip.

## 6. Acoustically Driven Microfluids Using SAW

Now we wish to introduce the basics that are necessary to understand the acoustic actuation scheme for SAW-driven fluid manipulation on a chip. We start with a short description of a SAW on a solid, as we employ SAWs to interact with a fluid, induce internal acoustic streaming or supply enough force to actuate a droplet as a whole. This SAW–fluid interaction is presented herein, with special emphasis given on the internal acoustic streaming in a small amount of fluid and droplet actuation on the other hand.

In a crystal, or more generally spoken in a solid, there exists a variety of optical and acoustic lattice vibrations. Already in 1885 the special case of SAWs has been described theoretically by Lord Rayleigh from the perspective of seismology.<sup>[64]</sup> SAWs are modes of elastic energy, which propagate on the surface of a substrate. Their energy is essentially confined to a layer thickness of about one wavelength. Today, SAW devices are widely used for radio-frequency (RF) signal processing and filter applications and became a huge industry in mobile communication. SAW devices have been around for years in communication circuitry—every cell phone has filters using the effect. An electrical signal fed into transducers on the surface of a piezoelectric chip is converted into a deformation of the crystal underneath. Given the right frequency of the signal, a mechanical wave is launched across the chip. In Figure 13, we sketch a snapshot of a SAW propagating on a solid. SAWs are especially easily excited on a piezoelectric solid. A set of interdigitated metal elec-

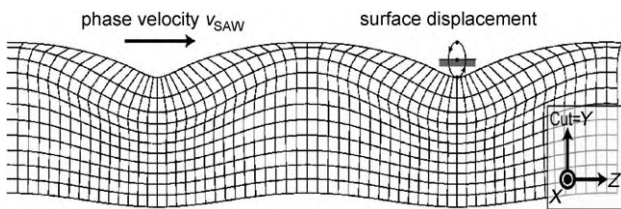


**Figure 13.** Sketch of a surface acoustic wave propagating on a piezoelectric substrate. Typical wavelengths are in the micrometer range, typical amplitudes less than a nanometer. Note the elliptically polarized displacement of the surface.

trodes on top of the surface acts as a transducer converting an RF electrical signal into a nearly monochromatic and coherent sound wave along the surface of the solid. The period of the fingers determines the frequency of the SAW, which depends on the SAW velocity of the given crystal orientation and cut, respectively. There are many different designs for such interdigital transducers (IDTs) for special purposes in high-frequency signal processing or sensor applications. Here, however, we only want to give an idea about their operation and therefore we restrict ourselves to the simplest cases. For fixed-frequency operation, an IDT consists of a comb-like metal structure where every second metal finger is connected. Application of an RF signal to the transducer causes a periodic crystal deformation underneath, via the inverse piezoelectric effect. In first order, the resonant frequency of such an IDT is then given by Equation (11):

$$f = \frac{v_{\text{SAW}}}{\lambda} \quad (11)$$

Here,  $\lambda$  denotes the periodicity of the IDT and  $v_{\text{SAW}}$  the velocity of the SAW along the crystal direction perpendicular to the IDT, that is, the direction of sound propagation.

The interaction between a SAW and a fluid on the surface of the substrate on which the SAW is propagating represents a delicate, though extremely interesting, hydrodynamical problem. To approach it, we, as usual for fluidic problems, first have to regard the Navier–Stokes equation [Eq. (5)], describing the flow in a hydrodynamic system.

To model the interaction between a SAW and a fluid, we treat the SAW as an array of point sources  $f_i$  of force, acting on a volume element of the fluid above the surface. This view is again justified, as it turns out that the fluid flow for the given length- and velocity-scales is overdamped. If the driving force is switched off, the flow ceases nearly immediately. Acoustic streaming in classical, macroscopic systems has been treated in detail by several authors in the past. For a detailed description, we wish to refer the reader to the works by Eckart<sup>[65]</sup> and Nyborg<sup>[66]</sup> as a starting point. The general framework of their theories on acoustic streaming is the following: The effect takes place on two separate time scales. On the short time scale, which in our case is the time scale of the SAW, the motion of the interface between the substrate and the fluid is resolved. On this scale, water does not perform an incompressible flow, but has to be described by the equations of compressible fluid dynamics which consider the mass–density of the fluid not as a constant, but as part of the problem. Compared to the stress tensor in the previously formulated Navier–Stokes equations, the stress then contains an additional term accounting for the compressibility. It is this compressibility that gives rise to higher-order terms in pressure and velocity, finally leading to a DC term in the pressure distribution and the acoustic streaming. They further rely on conservation of mass, and they relate density and pressure. The SAW, which is a wave on the substrate surface only, then causes a longitudinal sound wave propagating from the substrate into the fluid. This sound wave is subject to viscous damping along its path in

the fluid. Furthermore, the nonlinear terms in the compressible Navier–Stokes equation give rise to higher harmonic pressure and velocity fields, which oscillate at all multiples of the initial frequency. It turns out that due to phase matching arguments, the longitudinal sound wave in the fluid is obeying a diffraction law similar to the ones known from ray optics, leading to a diffraction of the wave from the parallel motion along the surface (SAW) to an oblique entrance into the fluid above the surface. The angle of diffraction is then given by the different sound velocities in the substrate and the fluid, respectively [Eq. (12)]:

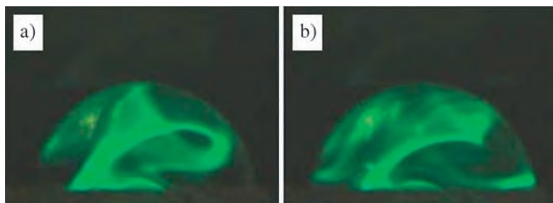
$$\sin(\theta_R) = \frac{v_{\text{fluid}}}{v_{\text{SAW}}} \quad (12)$$

This diffraction effect can easily be observed in an experiment, where a SAW-generating IDT is placed directly underneath a fluid reservoir, containing water and a small amount of ink to visualize the acoustic streaming in the container. In Figure 14, we depict the result of such an experiment.



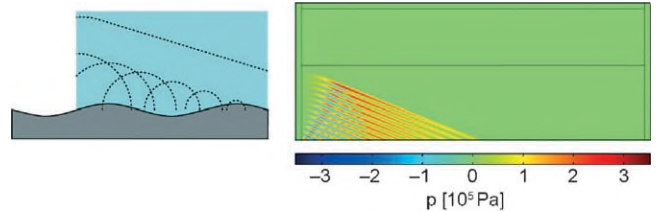
**Figure 14.** Fluid jets caused by an IDT at the bottom of a well covered by a small amount of dye. The fluid is contained in a cuvette, the part shown in the pictures is approximately 18 mm wide. Between the snapshots time spans of 0.16 s and 0.48 s have elapsed.

Figure 15 shows a similar experiment, this time performed in a small droplet. Here, a small amount of fluorescent dye is deposited on the surface of the chip, then a small droplet (approx. 50 nl) is pipetted onto this dye spot. A SAW impinging from the left quickly dissolves the dye and distributes it throughout the droplet. Apart from the beauty of these pictures, the experiment has an enormous impact for future biochips, as it indicates the possibility to dissolve chemical reagents in a small virtual test tube by means of a SAW. This would enable the manufacturer of the chip to ship it preloaded with reagents. Only a suitable buffer needs to be applied to the chip and the SAW-driven fluidics can do the rest.



**Figure 15.** SAW-induced internal acoustic streaming in a small droplet (typical volume: approximately 100 nl). To visualize the streaming, prior of the droplet deposition, a small amount of fluorescent dye had been deposited on the chip surface. The SAW impinging from the left quickly dissolves this dye.

This typical fingerprint of SAW-driven acoustic streaming can also be theoretically understood and visualized when we have a look at a finite element simulation of the pressure distribution in a SAW-driven fluid. If the SAW is modeled as an array of point sources for the forces  $f_i$  being attenuated into the direction of SAW propagation into the fluid reservoir, a Huygens-like superposition leads to plane waves in the fluid (Figure 16). Phase matching results in a Rayleigh angle  $\theta_R$ .



**Figure 16.** Finite element calculations of the pressure distribution in a substrate–fluid system as shown to the left in a simple Huygens-type model.<sup>[67]</sup>

## 7. SAW-Driven Acoustic Mixing

As can be already seen from Figure 15, SAW-induced acoustic streaming induces an internal liquid flow in small amounts of fluid. Although this effect still constitutes laminar flow, it can be exploited efficiently for acoustic mixing at small scales. A recent approach that we have been following in our laboratory relies on the folding of material flow lines by modulated SAW-induced streaming. Here, a SAW of a given frequency and direction with respect to the fluid volume is modulated either in space (trajectory) or in time. Each SAW induces a (stable) streaming pattern like the ones shown in Figures 14 or 15. When the SAW direction, frequency or amplitude is changed, this streaming pattern changes accordingly. Such SAW modulations can easily be achieved by switching the excitation parameters of the IDT.

One example for SAW mixing in a thin capillary gap formed between the SAW chip and a cover slip on top of it is shown in Figure 17. Here, we plot an experimentally obtained micrograph of a SAW spread dye in a capillary gap together with a theoretical calculation of the flow profile for the same geometry.<sup>[68]</sup> The experimental picture represents a snapshot some time after the SAW has been turned on. The inset of the right panel shows the time evolution of the shape as extracted from our model calculation. The lower part of the right panel exhibits a snapshot of the material folding or flow line after some time. Similar, but different flow lines are obtained if for example the direction of the SAW is changed. The resulting material distribution (dye in this case) then represents a superposition of the single quasi-static cases. If this procedure is repeated several times, a homogenous distribution of the dye is obtained.

More recently, we were also able to observe SAW-induced mixing in closed channels<sup>[69]</sup> and to trigger chaotic advection in a microfluidic system.<sup>[70]</sup> With this, we were able to predict optimum SAW propagation parameters to achieve perfect

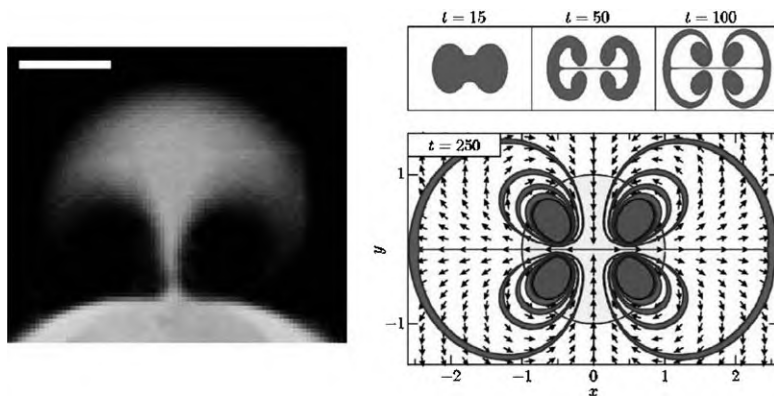


**Figure 17.** Left: A dye jet pumped by a SAW transducer, shortly after switching the RF power. In the center of the transducer, the fluid is pumped upwards; on both sides the fluid is sucked in. The bar is 0.5 mm wide. Right: Results of the theoretical modeling of this capillary gap flow profile. The inset shows the temporal evolution of the dye distribution.<sup>[68]</sup>

mixing after the shortest possible times for any given geometry (Figure 18).

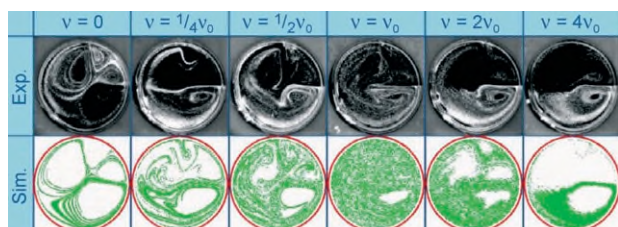


**Figure 18.** Experimental (top) and theoretical (bottom) visualization of SAW-induced acoustic mixing in a small reactor cell. The complex streaming patterns are achieved by superimposing two temporally modulated SAWs intruding into the fluid volume from the top and the right. The streaming patterns are made visible by tracer particles. Optimization of the relative modulation frequencies leads to a perfect mixing after shortest possible times, based on chaotic advection.<sup>[70]</sup>

There are many different applications for SAW-driven acoustic mixing in small fluid volumes. They range from micro-array hybridization<sup>[71]</sup> to protein arrays, in situ immunostaining, mixing in micro-titer plates and in cuvettes for optical investigation of fluids, including the extraction of blood parameters. This technique has recently been commercialized and many application notes and devices based on the SAW driven mixing can be found at <http://www.Advalytix.de>.

## 8. SAW-Driven Droplet Actuation

In Section 7, we reported on SAW-based acoustic mixing, which originates from acoustic streaming within small fluid volumes while interacting with SAWs. This acoustic streaming requires only very small SAW amplitudes as the SAW–fluid interaction is a very prominent effect. However, if the SAW amplitude is somewhat increased, the acoustic streaming may lead to a deformation of the liquid surface of free droplets on the surface, and eventually to a SAW-induced movement of such a droplet as a whole. If the chip surface is additionally

chemically patterned, the SAW can be used to actuate the droplet along those predetermined trajectories. In this sense, the droplet really acts as a virtual test tube that can be transported to some predetermined position on the chip, merged with other droplets, and so forth. As the chip is produced completely by employing semiconductor processing technologies, almost any desired “real estate” can be implemented on the chip, such as heaters and sensors. One example of such a multifunctional chip is shown in Figure 19. Here, we depict a

bird’s eye view of an approximately  $8 \times 8 \text{ mm}^2$  chip containing a number of different SAW generators (IDTs), a heater and a thermometer in its center. Three droplets can independently be actuated on this chip. The series of pictures is only meant to elucidate the function of the chip. Once merged and acoustically mixed, the two droplets undergo a chemical reaction leading, in this case, to a color change.

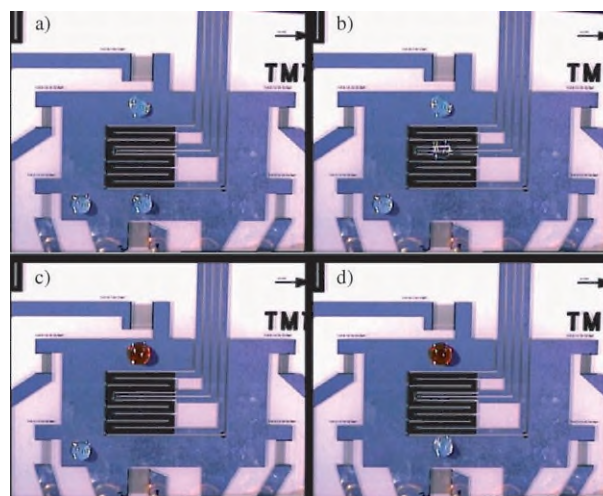


**Figure 19.** A SAW-driven microfluidic processor. Three droplets (approx. 100 nl each) are moved, remotely and independently controlled by the nanopumps; a)–d) represent a series of snapshots taken subsequently to visualize the movement, and the nanochemical reactions occurring when the droplets are merged and mixed by the action of the surface wave. The chip not only contains the nanopumps and the fluidic environment, but also additional real estate such as sensors and heaters.

As a prominent example for the versatility of SAW-driven, droplet-based microfluidic technology, we would like to refer the reader to our recent investigations of a chip laboratory where submicroliter polymerase chain reaction (PCR) was successfully demonstrated.<sup>[72]</sup> We are currently working on a complex chip system for single-cell cytogenetic investigations and analysis based on PCR and micro-array detection.

## 9. Blood Flow on a Chip

Up to now, we have highlighted some of the basic properties of SAW-driven microfluidic technology and hope to have triggered the imagination of the readership. The technique has only been in existence for a few years, but already there have been many different applications, as shown by the references. To conclude this overview, we discuss at least one of the applications in greater detail, namely the simulation of an artificial blood vessel, and the role of a biopolymer for the early stages of blood clotting. For this purpose, we need to give a few introductory details.

The complex geometry of our micro-vascular system ensures both sufficient supplies of nutrients (oxygen, etc.) as well as the effective removal of waste. In order to reach our entire body, the vessel system is devised as an architecture of branched capillaries in the neighborhood of literally every cell. The active surface of our vessel system (arteries, arterioles and capillaries) is comparable to the size of an entire soccer field ( $\sim 5000 \text{ m}^2$ ). The inner lining of the system is coated with endothelial cells whose surfaces are the key for blood transport and supply of all important organs. Typical diameters found in the microcirculatory system range between  $10 \mu\text{m}$ – $100 \mu\text{m}$ . Therefore, the hydrodynamic laws in this system are found in the world of micro-fluidics and vary significantly from our daily experience in the macroscopic world.

The forces acting on our vessel walls are mainly characterized by the shear flow created by the interaction between the blood and the adjacent vessel surface. Typically, we find shear rates between  $1000 \text{ s}^{-1}$  (capillaries) and  $8000 \text{ s}^{-1}$  (arterioles).<sup>[73]</sup> These rates can create forces which result in tiny fractures in our fragile vessel walls. The consequences are small bleedings (petechiae), which have to be sealed immediately. 50 years ago people found that the substance responsible for the sealing process is a protein called “von Willebrand factor” (VWF). It binds to the vessel wall, forms networks and binds free-floating blood platelets especially efficiently under high shear rates,<sup>[74–76]</sup> which appears quite counterintuitive. The blood platelets accumulate under high shear, seal the damaged vessel wall and therefore stop the bleeding. This process is the initial step of an entire cascade of blood clotting.

In 1926 Erik Adolf von Willebrand, a Finnish physician, reported a bleeding disorder he called hereditary pseudo-hemophilia. In contrast to the already known hemophilia A (a lack in factor VIII, only X-chromosomal), von Willebrand has found the bleeding disorder in both male and females of the same family, leading to the conclusion that it must have a different genetic cause. A while later the missing clotting factor was identified and it was named VWF after its founder. Only a few years later the first therapies substituting VWF were started.

VWF is found in the subendothelial matrix as well as in plasma ( $\sim 10 \mu\text{g mL}^{-1}$ ), where its most important function is the adhesion and aggregation of blood platelets via the glycoprotein (GP) binding site.<sup>[74,75]</sup> Importantly, only VWF is capable to capture platelets under high (arterial) shear rates. A disease known as von Willebrand–Jürgens syndrome, caused by a lack of blood-clotting factors, is one of the most common heredita-

ry illnesses known. However the majority of the patients are non-symptomatic and are therefore not diagnosed.

Over the past few years VWF research experienced an exciting increase. Experiments showed that VWF can form up to 1 mm long fibers after being released from the endothelial cells (EC). These fibers adhere to the EC surface and immobilize blood platelets<sup>[78]</sup> (Figure 20). Structure and function were

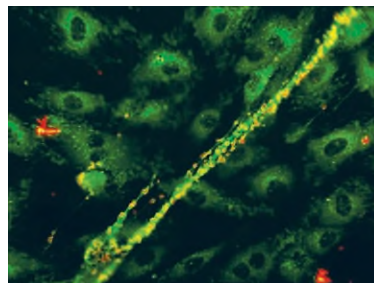


**Figure 20.** After stimulation of endothelial cells (green cells in the backgrounds), an approximately  $400 \mu\text{m}$  long VWF thread (green, from left bottom to the top right) is released at the luminal endothelium surface. This VWF thread binds platelets (red) under the influence of shear.

shown to be clearly correlated—the longer the fiber, the better it seems to bind platelets. At the same time, degradation increases with length. Lacking the enzyme in charge for VWF degradation leads to ultra-large fibers of VWF circulating in the blood (Figure 20). These fibers can bind platelets, which causes uncontrolled clotting and a deficiency in platelet concentration. Multiple little infarcts and petechial bleedings are the consequences of the thrombocytopenia. However, the mechanism that leads to the formation of these ultralarge fibers under high shear rates as well as the efficient way VWF is set into action under these conditions, remained entirely unclear until recently. In order to study this phenomenon in detail, a suitable in vitro model, mimicking flow profiles and forces of our microcirculatory system, was necessary.

An in vitro model for the study of blood flow phenomena, however, places particular demands on the technology used. Especially when it comes to the dynamics of polymers under the influence of shear, a microfluidic scheme to produce a controlled flow and shear is essential. Moreover, a natural mimicking of the shape and function of the blood vessels and the physiological conditions on the chip are vital ingredients, as are good accessibility for analytical procedures by optical methods.

An example of such an artificial blood vessel is shown in Figure 21, where we depict the fluidic part of one of our SAW-driven chips. Employing photolithography, we are able to define hydrophilic lanes on the chip having dimensions and branchings comparable to a real blood vessel. The only difference is that we are dealing with a flat and planar version of a channel, as described above. Apart from superior performance in terms of microfluidics, it has also the advantage to be easily accessible from the outside, either to load it with appropriate fluids and reagents, or to inspect and monitor the fluid dynamics using fluorescence microscopy. The interdigitated transduc-

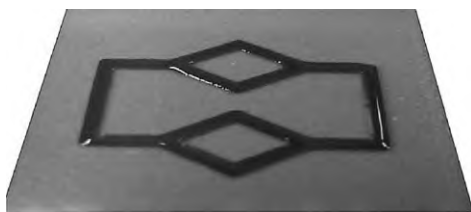


**Figure 21.** Example of a microliter flow chamber (sample volume approximately 10  $\mu\text{L}$ ) with lithographically defined bifurcations. The liquid is laterally confined to the chip surface by means of a hydrophobic/hydrophilic surface functionalization and being actuated by a SAW, which in turn is generated by a transducer (not shown) on a piezoelectric substrate.

ers to excite the SAW are not shown in this figure. The surface wave amplitude and the geometry determine the achievable flow velocities and shear.

Figure 22 displays one of the key results of our investigation. Under the influence of a well-defined and relatively sharp threshold shear ( $\sim 3000 \text{ s}^{-1}$ ), we find a sudden transition from a collapsed (left) into a stretched state (right).<sup>[77]</sup> This process is reversible, unless the protein finds an exposed binding site and comes to adhesion. To study the relationship between the conformation of the protein and the adhesion to a damaged vessel wall (conformation–functional relationship), we coated the microfluidic channel with collagen. In our blood vessels, collagen lies directly below the endothelium, and in the case of a vascular injury, it is directly accessible to the blood stream. Our channel functionalization thus simulates a vessel injury.

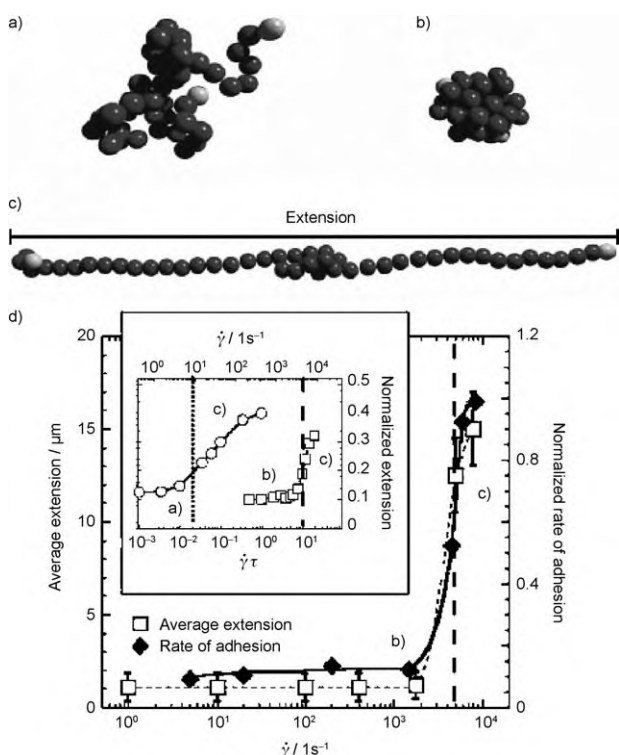


**Figure 22.** Average polymer extension (left scale) and normalized rate of adhesion (right scale) for VWF in a SAW-driven microfluidic shear field.<sup>[45]</sup> Upon being subjected to a well-defined shear force, the VWF unfolds and exposes specific binding sites, thus increasing the rate of adhesion.

The results of our experiments shed new light onto the VWF biopolymer, because according to the present understanding of the activation of the protein could also occur in intact, non-injured vessels. At high enough shear rates VWF could be discharged into the blood, stretched and thus be ready to bind. Thus, nature found a unique way to ensure that a life-threatening situation is always under strict control. These new insights in fact permit many researchers to view vascular diseases in a new, medical–physical light, which should soon result novel therapeutic approaches. Even for inflammations and tumor metastasis, the activation of the VWF could play a crucial role.<sup>[79,80]</sup> We are convinced that further insights into the structure and behavior of this fascinating molecule will also lead to exciting and most interesting insights into the transport system blood.

In summary, our aim was to give an overview—definitely not comprehensive—of the difficulties and hurdles that scaling down a fluidic system to the micro- or nanometer range bring along, and to depict a few examples on how these difficulties are tackled technologically.

The field of microfluidics is very active and new discoveries and technological improvements are emerging on a nearly daily basis. We are well aware of the fact that we might have omitted some of the smartest ideas and solutions, but including all of them would be beyond our capabilities herein. Instead, we spent some time and efforts to explain and describe our own technology, where we actuate very small amount of fluids on the planar surface of a piezoelectric chip.

We use SAWs to induce acoustic streaming in a small fluid volume. This is electrically controllable as the SAWs are excited by an RF signal to the transducers. At low SAW powers, efficient mixing is achieved, especially while spatially and temporally modulating the SAW and hence the interaction with the fluid. Quasi-chaotic advection with salient mixing capabilities was demonstrated. At higher powers, SAWs are able to actuate a small fluid volume (either as droplet or within a closed channel geometry). This way, a programmable fluidic microprocessor can be envisioned. As an example for such a complex microfluidic system we described our efforts to realize a PCR chip for sub-microliter sample volumes. The shear force fields generated in the fluid under the action of a SAW together with their pumping action was used to simulate blood vessels and blood flow on a chip. We cultivated a cell floor on the microfluidic chip and to investigate the adhesion properties of blood platelets initiated by the SAW-mediated mechanical activation of a biopolymer (von Willebrand factor). Here, too, the programmability of SAW-mediated streaming together with surface functionalization proved to be very useful for the microfluidic application presented. For instance, we could show unambiguously that the binding rate is strongly dependent on the conformational changes and nature of this biopolymer and thus we contributed to a better understanding of the initial stages of blood clotting.

We hope that we were able to demonstrate that there are many great ideas and realizations in the vastly growing field of microfluidics leading to a true lab-on-a-chip. The simplicity, the ease of construction and the planar integration of reaction ves-

sels, “tubing” and even the pumps and/or mixers makes the SAW-driven microfluidic approach especially promising. The low price of our chips makes them ideally suited to serve as consumables, and we are hence quite convinced that they might make it into the doctor’s office for point-of-care diagnostic applications in the not-too-distant future.

However, we were unable to cover the whole range of experimental and theoretical work that was done in the last few years since we have had the pleasure to work in this field. From this, it also becomes clear that our own work is the result of the efforts of many colleagues from many different disciplines as partially named in the references and in the acknowledgments.

## Acknowledgements

We would like to thank a few colleagues personally, without whom a lot of the experiments that we presented would have been impossible. First, we like to thank Matthias Schneider (biophysicist in Augsburg) and his brother Stefan (physician and Professor of Medicine in Münster, Germany) for the fabulous work on the von Willebrand factor and blood vessels on a chip. Stefan Thalhammer (biologist, Helmholtz center in Munich, Germany) supplied much of the technological overview and triggered a wealth of new ideas and technological solutions, especially in the field of cytogenetics. Thomas Frommelt (physicist) became obsessed with the art of SAW-driven mixing during his PhD in Augsburg. Jürgen Scriba and Christoph Gauer (both physicists) made the commercialization possible by co-founding Advalytix AG, Munich. Peter Hänggi, Peter Talkner and Michael Schindler (theoretical physicists in Augsburg) and Daniel Köster, Roland Hoppe and Kunibert Siebert (applied mathematicians in Augsburg) were a great team with whom to work and to discuss our experimental findings. This work has been financially supported in part by the Deutsche Forschungsgemeinschaft (SFB 486, SFB 492, SPP 1164), in part also by the Cluster of Excellence “Nano Systems Initiative Munich”, (NIM), and partly through the Elite Network Bavaria (Complnt) and the “Innovative Medical Research Program at the University of Münster. We also thank the Bayerische Forschungsförderung for financial support under the programs FORNANO and FOROXID, as well as a grant entitled “Programmable cytogenetic sub-microliter lab-on-a-chip”. Finally, we thank the Center for Nanoscience at the LMU in Munich, the University of Augsburg and Olympus Advalytix, Munich for constant support.

**Keywords:** materials science · mechanical properties · microfluidic flow chamber · proteins · surface acoustic waves

- [1] E. M. Purcell, *Am. J. Phys.* **1977**, *45*, 3–11.
- [2] J. G. Smits, *Sens. Actuators A* **1990**, *21–23*, 203–206.
- [3] A. Manz, C. S. Effenhauser, N. Burggraf, D. J. Harrison, K. Seiler, K. Fluri, *J. Micromech. Microeng.* **1994**, *4*, 257–265.
- [4] G. P. Lopez, H. A. Biebuyck, C. D. Frisbie, G. M. Whitesides, *Science* **1993**, *260*, 647–649.
- [5] G. Möller, M. Harke, H. Motschmann, *Langmuir* **1998**, *14*, 4955–4957.
- [6] H. Gau, S. Herminghaus, P. Lenz, R. Lipowski, *Science* **1999**, *283*, 46–49.
- [7] S. Daniel, M. K. Chaudhury, J. C. Chen, *Science* **2001**, *291*, 633–636.
- [8] K. Ichimura, S. K. Oh, M. Nakagawa, *Science* **2000**, *288*, 1624–1626.
- [9] R. M. Moroney, R. M. White, R. T. Howe, *Appl. Phys. Lett.* **1991**, *59*, 774–776.
- [10] M. A. Unger, H. P. Chou, T. Thorsen, A. Scherer, S. R. Quake, *Science* **2000**, *288*, 113–116.
- [11] L. D. Landau, E. M. Lifschitz, *Fluid Mechanics, Vol. 6*, Pergamon Press, Oxford, **1987**.
- [12] E. Guyon, J.-P. Hulin, L. Petit, C. D. Matescu, *Physical Hydrodynamics*, Oxford University Press, Oxford, **2001**.
- [13] P. Tabeling, *Introduction to Microfluidics*, Oxford University Press, Oxford, **2005**.
- [14] H. A. Stone, A. D. Stroock, A. Ajdari, *Annu. Rev. Fluid Mech.* **2004**, *36*, 381–411.
- [15] T. M. Squires, S. R. Quake, *Rev. Mod. Phys.* **2005**, *77*, 977–1026.
- [16] A. E. Kamholz, B. H. Weigl, B. A. Finlayson, P. Yager, *Anal. Chem.* **1999**, *71*, 5340–5347.
- [17] R. F. Ismagilov, A. D. Stroock, P. J. A. Kenis, G. Whitesides, H. A. Stone, *Appl. Phys. Lett.* **2000**, *76*, 2376–2378.
- [18] J. P. Brody, P. Yager, R. E. Goldstein, R. H. Austin, *Biophys. J.* **1996**, *71*, 3430–3441.
- [19] J. P. Brody, P. Yager, *Sens. Actuators A* **1997**, *58*, 13–18.
- [20] B. S. Cho, T. G. Schuster, X. Zhu, D. Chang, G. D. Smith, S. Takayama, *Anal. Chem.* **2003**, *75*, 1671–1675.
- [21] H. Song, J. D. Tice, R. F. Ismagilov, *Angew. Chem.* **2003**, *115*, 792–796; *Angew. Chem. Int. Ed.* **2003**, *42*, 768–772.
- [22] D. R. Link, S. L. Anna, D. A. Weitz, H. A. Stone, *Phys. Rev. Lett.* **2004**, *92*, 054503.
- [23] A. S. Utada, L. Y. Chu, A. Fernandez-Nieves, D. R. Link, C. Holtze, D. A. Weitz, *MRS Bull.* **2007**, *32*, 702–708.
- [24] A. S. Utada, A. F. Fernandez-Nieves, H. A. Stone, D. A. Weitz, *Phys. Rev. Lett.* **2007**, *99*, 094502.
- [25] A. S. Utada, E. Lorenceau, D. R. Link, P. D. Kaplan, H. A. Stone, D. A. Weitz, *Science* **2005**, *308*, 537–541.
- [26] L.-Y. Chu, A. S. Utada, R. K. Shah, J.-W. Kim, D. A. Weitz, *Angew. Chem.* **2007**, *119*, 9128–9132; *Angew. Chem. Int. Ed.* **2007**, *46*, 8970–8974.
- [27] S. L. Anna, N. Bontoux, H. A. Stone, *Appl. Phys. Lett.* **2003**, *82*, 364–366.
- [28] R. K. Shah, H. C. Shum, A. C. Rowat, D. Lee, J. J. Agresti, A. S. Utada, L.-Y. Chu, J.-W. Kim, A. Fernandez-Nieves, C. J. Martinez, D. A. Weitz, *Mater. Today* **2008**, *11*, 18–27.
- [29] M. Brinkmann, R. Lipowsky, *J. Appl. Phys.* **2002**, *92*, 4296–4306.
- [30] R. Lipowsky, M. Brinkmann, R. Dimova, T. Franke, J. Kierfeld, X. Zhang, *J. Phys. Condens. Matter* **2005**, *17*, S537–S558.
- [31] A. Klingner, F. Mugele, *J. Appl. Phys.* **2004**, *95*, 2918–2920.
- [32] N. Xia, T. P. Hunt, B. T. Mayers, E. Alsborg, G. M. Whitesides, R. M. Westervelt, D. E. Ingber, *Biomed. Microdevices* **2006**, *8*, 299–308.
- [33] S. S. Shevkoplyas, A. C. Siegel, R. M. Westervelt, M. G. Prentiss, G. M. Whitesides, *Lab Chip* **2007**, *7*, 1294–1302.
- [34] C. Wilhelm, F. Gazeau, J.-C. Bacri, *Phys. Rev. E* **2003**, *67*, 061908.
- [35] C. Wilhelm, J. Browaeys, A. Ponton, J.-C. Bacri, *Phys. Rev. E* **2003**, *67*, 011504.
- [36] C. S. Lee, H. Lee, R. M. Westervelt, *Appl. Phys. Lett.* **2001**, *79*, 3308–3310.
- [37] H. Lee, Y. Liu, D. Ham, R. M. Westervelt, *Lab Chip* **2007**, *7*, 331–337.
- [38] A. Manz, N. Graber, H. M. Widmer, *Sens. Actuators B* **1990**, *1*, 244–248.
- [39] A. Manz, Y. Miyahara, J. Miura, Y. Watanabe, H. Miyagi, K. Sato, *Sens. Actuators B* **1990**, *1*, 249–255.
- [40] P. Wilding, M. A. Shoffner, L. J. Kricka, *Clin. Chem.* **1994**, *40*, 1815–1818.
- [41] D. J. Harrison, K. Fluri, K. Seiler, Z. Fan, C. S. Effenhauser, A. Manz, *Science* **1993**, *261*, 895–897.
- [42] L. Martynova, L. E. Locascio, M. Gaitan, G. W. Kramer, R. G. Christensen, W. A. MacCrehan, *Anal. Chem.* **1997**, *69*, 4783–4789.
- [43] D. C. Duffy, J. C. McDonald, O. J. A. Schueller, G. M. Whitesides, *Anal. Chem.* **1998**, *70*, 4974–4984.
- [44] Y. Xia, G. M. Whitesides, *Angew. Chem.* **1998**, *110*, 568–594; *Angew. Chem. Int. Ed.* **1998**, *37*, 550–575.
- [45] S. W. Schneider, S. Nuschele, A. Wixforth, C. Gorzelanny, A. Alexander-Katz, R. R. Netz, M. F. Schneider, *Proc. Natl. Acad. Sci. USA* **2007**, *104*, 7899–7903.
- [46] T. Thorsen, S. J. Maerkl, S. R. Quake, *Science* **2002**, *298*, 580–584.
- [47] A. Khademhosseini, J. Yeh, S. Y. Jon, G. Eng, K. Y. Suh, J. Burdick, R. Langer, *Lab Chip* **2004**, *4*, 425–430.
- [48] H. Andersson, A. van den Berg, *Lab Chip* **2004**, *4*, 98–103.
- [49] W. C. Chang, L. P. Lee, D. Liepmann, *Lab Chip* **2005**, *5*, 64–73.

- [50] N. T. Nguyen, X. Y. Huang, T. K. Chuan, *J. Fluids Eng.* **2002**, *124*, 384–392.
- [51] P. M. White, *Fluid Mechanics*, McGraw Hill, New York, **1986**.
- [52] C. H. Ahn, M. G. Allen, *Fluid Micropumps Based on Rotary Magnetic Actuators*, IEEE 8th Int. Workshop on MEMS (MEMS'95), **1995**, 408–412.
- [53] J. Doepper, M. Clemens, W. Ehrfeld, S. Jung, K. P. Kaemper, H. Lehr, *J. Micromech. Microeng.* **1997**, *7*, 230–232.
- [54] S. Haeberle, T. Brenner, R. Zengerle, J. Ducree, *Lab Chip* **2006**, *6*, 776–781.
- [55] Z. Yang, S. Matsumoto, H. Goto, M. Matsumoto, R. Maeda, *Sens. Actuators A* **2001**, *93*, 266–272.
- [56] R. M. Moroney, R. M. White, R. T. Howe, *IEEE 4th Int. Workshop on MEMS (MEMS '91)* **1991**, 277–282.
- [57] N. T. Nguyen, A. H. Meng, J. Black, R. M. White, *Sens. Actuators A* **2000**, *79*, 115–121.
- [58] M. Kurosawa, T. Watanabe, T. Higuchi, *IEEE 8th Int. Workshop on MEMS (MEMS'95)* **1995**, 25–30.
- [59] A. Wixforth, *Superlattices Microstruct.* **2003**, *33*, 389–396.
- [60] S. Shoji, M. Esashi, *J. Micromech. Microeng.* **1994**, *4*, 157–171.
- [61] S. Haeberle, R. Zengerle, *Lab Chip* **2007**, *7*, 1094–1110.
- [62] S. F. Bart, L. S. Tavrow, M. Mehregany, J. H. Lang, *Sens. Actuators A* **1990**, *21–23*, 193–197.
- [63] G. Fuhr, T. Schnelle, B. Wagner, *J. Micromech. Microeng.* **1994**, *4*, 217–226.
- [64] L. Rayleigh, *Proc. London Math. Soc.* **1885**, *17*, 4–11.
- [65] C. Eckart, *Phys. Rev.* **1948**, *73*, 68–77.
- [66] W. L. Nyborg in *Physical Acoustics 2B* (Ed.: W. P. Mason), Academic Press, San Diego, **1965**, p. 265.
- [67] T. Frommelt, *PhD Dissertation*, University of Augsburg, **2007**.
- [68] Z. Guttenberg, A. Rathgeber, S. Keller, J. O. Rädler, A. Wixforth, M. Kostur, M. Schindler, P. Talkner, *Phys. Rev. E* **2004**, *70*, 056311.
- [69] K. Sritharan, C. J. Strobl, M. F. Schneider, A. Wixforth, Z. Guttenberg, *Appl. Phys. Lett.* **2006**, *88*, 054102.
- [70] T. Frommelt, M. Kostur, M. Wenzel-Schäfer, P. Talkner, P. Hänggi, A. Wixforth, *Phys. Rev. Lett.* **2008**, *100*, 034502.
- [71] A. Toegl, R. Kirchner, C. Gauer, A. Wixforth, *J. Biomol. Techniques* **2003**, *14*, 197–204.
- [72] Z. Guttenberg, H. Müller, H. Habermüller, A. Geisbauer, J. Pipper, J. Felbel, M. Kielpinski, J. Scriba, A. Wixforth, *Lab Chip* **2005**, *5*, 308–317.
- [73] G. A. Trusky, F. Yuan, D. F. Katz, *Transport Phenomena in Biological Systems*, Pearson, New Jersey, **2004**.
- [74] Z. M. Ruggeri, *Best Pract. Res. Clin. Haematol.* **2001**, *14*, 257–279.
- [75] Z. M. Ruggeri, *Thromb. Haemostasis* **2007**, *98*, 55–62.
- [76] R. Schneppenheim, *Blood Coagulation Fibrinolysis* **2005**, *16*, S3–S10.
- [77] A. Alexander-Katz, M. F. Schneider, S. W. Schneider, A. Wixforth, R. R. Netz, *Phys. Rev. Lett.* **2006**, *97*, 138101.
- [78] T. Goerge, F. Kleinerüschkamp, A. Barg, E.-M. Schnaeker, V. Huck, M. F. Schneider, M. Steinhoff, S. W. Schneider, *Thromb. Haemostasis* **2007**, *98*, 283–286.
- [79] V. Terraube, R. Pendu, D. Baruch, M. F. Gebbink, D. Meyer, P. J. Lenting, C. V. Denis, *J. Thromb. Haemostasis* **2006**, *4*, 519–526.
- [80] D. D. Wagner, *Arterioscler. Thromb. Vasc. Biol.* **2005**, *25*, 1321–1324.